Soil Dynamics and Earthquake Engineering xxx (xxxx) xxx–xxx

Contents lists available at ScienceDirect

Soil Dynamics and Earthquake Engineering

journal homepage: www.elsevier.com/locate/soildyn

Degree of saturation affecting liquefaction resistance and undrained shear strength of silty sands

Yoshimichi Tsukamoto*

Department of Civil Engineering, Tokyo University of Science, 2641, Yamazaki, Noda City, Chiba 278-8510, Japan

A B S T R A C T

The undrained shear strength and liquefaction cyclic resistance of silty sands are examined based on a large number of laboratory triaxial test results. The influence of saturation on the liquefaction triggering and occurrence of liquefaction-induced flow slides is highlighted. The laboratory triaxial tests are conducted separately in the three phases of full saturation, partial saturation and unsaturation. The past studies of the authors' are first reviewed and some new data are added where appropriate. The different responses of silty sands in those three phases of saturation are discussed in detail.

1. Introduction

The liquefaction resistance and undrained shear strength of soils are the key parameters to determine the liquefaction triggering and liquefaction-induced flow slides of earth structures during earthquakes. This paper is aimed at highlighting the influence of saturation on the liquefaction resistance and undrained shear strength of silty sands, based on laboratory triaxial test results. In this paper, the phases of saturation in soils are separated into three categories, full saturation, partial saturation and unsaturation. It is known from the observation of field velocity logging tests that a velocity of propagation of primary wave of approximately 1600 m/s is observed in soil layers far below a groundwater level, indicating that these soil layers are fully saturated. However, it is also known that there is a soil layer of 3–5 m deep immediately below a groundwater level that typically exhibits a velocity of propagation of primary wave of 500–1000 m/s, implying that this soil layer is partially saturated with pore water containing some minute air bubbles. On the other hand, there is a soil layer immediately above a groundwater level, where capillary water rises up through soil aggregates and a negative pore water pressure develops relative to an atmospheric air pressure, due to surface tension of pore water, leading to development of capillary suction within soil aggregates. Fig. 1 illustrates conceptually the phase transformation of saturation in soils in a diagram of pore air and pore water pressures, u_a & u_w, against confining stress σ, based on the work of Fredlund and Rahardjo [1]. When soils are unsaturated, though nearly saturated under an atmospheric pressure, there would be some continuous air phases within soil aggregates, where the matric suction of $s_u = u_a - u_w$ would be present due to surface tension of pore water within soil aggregates. The surface tension tends to interact with soil aggregates and to produce bonds of soil structures, and therefore is likely to mobilise shear strength of soils. When soils experience some increase in the confining stress σ, the pore air and pore water pressures would also increase, where the coefficients of pore air and pore water pressures can be defined as $B_a = \Delta u_a/\Delta\sigma$ and $B_w = \Delta u_w/\Delta\sigma$. These two parameters take different values and are lower than 1 due to surface tension of pore water within soil aggregates. However, the matric suction gradually reduces as the confining stress increases. There would then be a phase transformation from unsaturation to partial saturation, where the continuous air phases within soil aggregates eventually fade away and the matric suction becomes negligible. Instead, the occluded air bubbles would become prevalent within pore water. These tiny air bubbles existing primarily within pore water would not markedly interact with soil aggregates, though they would alter the compressibility of pore water. There would then be only one coefficient of pore water pressure B, which is lower than 1 in the phase of partial saturation. When the confining stress increases further, these occluded air bubbles would eventually diminish leading to the pore water being virtually incompressible and the coefficient of pore water pressure B being equal to 1.

The coefficient of pore water pressure B is used to illustrate the phase transformation of soils from full saturation to partial saturation, as shown in Fig. 1. However, the degree of saturation S_r is the most widely used parameter to define the overall changes of saturation in soils. The relation between these two parameters was described by Kamata et al. [2] and given as follows,

* Corresponding author.
E-mail address: ytsoil@rs.noda.tus.ac.jp.

https://doi.org/10.1016/j.soildyn.2018.04.041
Received 8 August 2017; Received in revised form 2 March 2018; Accepted 25 April 2018
0267-7261/

Please cite this article as: Tsukamoto, Y., Soil Dynamics and Earthquake Engineering (2018), https://doi.org/10.1016/j.soildyn.2018.04.041

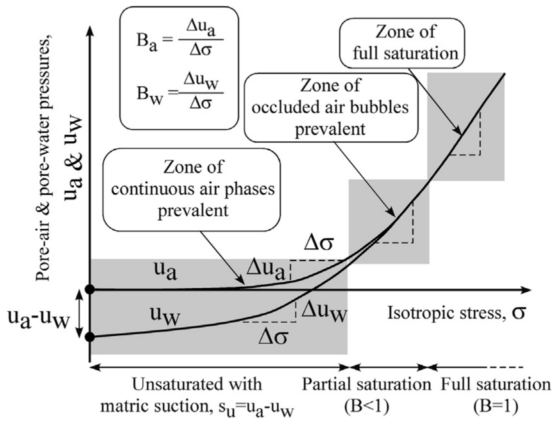

Fig. 1. Confining stress – pore pressure relations in soils.

$$S_r = \frac{C_a - \frac{C_b(1-B)}{nB^2}}{C_a - C_w} = \frac{C_a - \frac{3}{2G_o n}\frac{1-2\nu_b}{1+\nu_b}\frac{1-B}{B^2}}{C_a - C_w} \tag{1}$$

where C_a, C_w and C_b are the compressibility of pore air, pore water and soil skeleton, n is the porosity, G_o is the initial shear modulus and ν_b is the skeleton Poisson's ratio. The relation between the values of S_r and B is shown in Fig. 2, where the typical values of C_a, C_w, C_b, n, G_o and ν_b are assumed. It is found in Fig. 2 that the value of B changes widely from 1 to 0.1 in response to the change of S_r from 100% to 80%, and is found to serve as a good parameter to express the change of saturation in the phase of partial saturation. On the other hand, the value of S_r changes widely from 80% to 0% in response to the change of B from 0.1 to the lowest, and is found to serve as a good parameter to express the change of saturation in the phase of unsaturation.

In this study, the liquefaction resistance and undrained shear strength of silty sands are reviewed from the authors' past studies and reexamined by adding some new data where appropriate. Those studies are exclusively based on laboratory triaxial tests conducted separately in the different phases of full saturation, partial saturation and unsaturation. The physical properties of all the soils examined in this study are summarised in Table 1.

2. Review of undrained shear strength and liquefaction resistance of saturated silty sands

The undrained shear strength of saturated silty sands has been extensively examined in the past studies, based on laboratory triaxial tests. Those studies were primarily based on the context of a steady

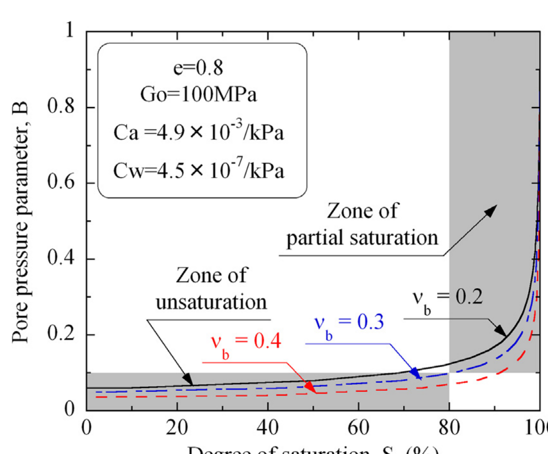

Fig. 2. Relation between degree of saturation S_r and coefficient of pore water pressure B.

Table 1
Physical properties of soils.

Soil	ρ_s (g/cm^3)	F_c (%)	D_{50} (mm)	e_{max}	e_{min}
Toyoura sand	2.657	0	0.17	0.973	0.607
Jamuna river sand	2.745	15.5	0.19	1.202	0.602
Omigawa sand	2.694	8.4	0.17	1.282	0.796
Inagi sand	2.726	26.9	0.16	1.803	1.023
Koshigaya sand	2.69	1–27	0.22–0.40	1.06–1.19	0.71–0.88
Takenouchi silt	2.65	89–99	0.03–0.05	2.01–2.40	1.12–1.32

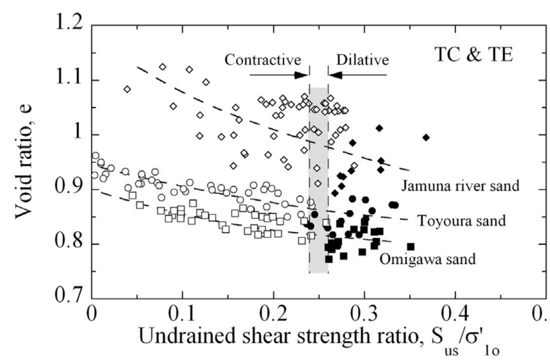

Fig. 3. Plots of saturated undrained shear strength ratio S_{us}/σ'_{1o} against void ratio e (data after Tsukamoto et al., 2009).

state concept, and the relations of shear stress and strain were characterized by the contractive behaviour and dilative behaviour, corresponding to the distinction of "flow" and "no flow". The contractive behaviour corresponds to the condition of "flow", where the shear stress increases and then begins to reduce, as the positive pore water pressure is developed. The dilative behaviour corresponds to the condition of "no flow", where the shear stress continues to increase as the development of positive and then negative pore water pressure occurs. Fig. 3 shows the plots of the undrained shear strength ratio S_{us}/σ'_{1o} against void ratio e for Toyoura clean sand, Jamuna river silty sand and Omigawa silty sand, where S_{us} is the undrained shear strength and σ'_{1o} is the initial major effective stress. The data on the undrained triaxial compression and extension tests are included. It is found that the relations between the undrained shear strength and density differ significantly among the soils investigated. In the previous study of Tsukamoto et al. [3], the same set of data was also presented in terms of relative density D_r plotted against the undrained shear strength ratio. It was noted then that the values of S_{us}/σ'_{1o} dividing contractive and dilative behaviour are 0.24–0.26 and rather constant regardless of soils, though the corresponding values of D_r differ significantly. It is to note here that in calculating the relative density D_r, the maximum and minimum void ratios of e_{max} and e_{min} were determined by the testing methods stipulated by JGS [4]. Following the recent innovation and developments on the concept of skeleton void ratio and similar concepts, it would be worthwhile to reexamine the relations of the undrained shear strength and density in the context of skeleton void ratio to achieve its unique relationship.

Fig. 4(a) shows the plots of the liquefaction resistance R_l against relative density D_r for clean sands, which were obtained from laboratory undrained cyclic triaxial tests. It is known that the linear relation tends to hold in the range of D_r lower than 80%. In Fig. 4(b), the same plots for silty sands are indicated. It is again to note here that the values of e_{max} and e_{min} were determined by the testing methods of JGS [4] to calculate the values of D_r. It is found that there is a range of D_r lower than about 25%, where there are no data available, implying that there could be the lowest limit of D_r as long as the values of D_r were calculated from the values of e_{max} and e_{min} based on JGS [4]. It is to note here that when silty sand samples are saturated and subjected to a confining stress, the void ratios of those samples tend to exhibit lower

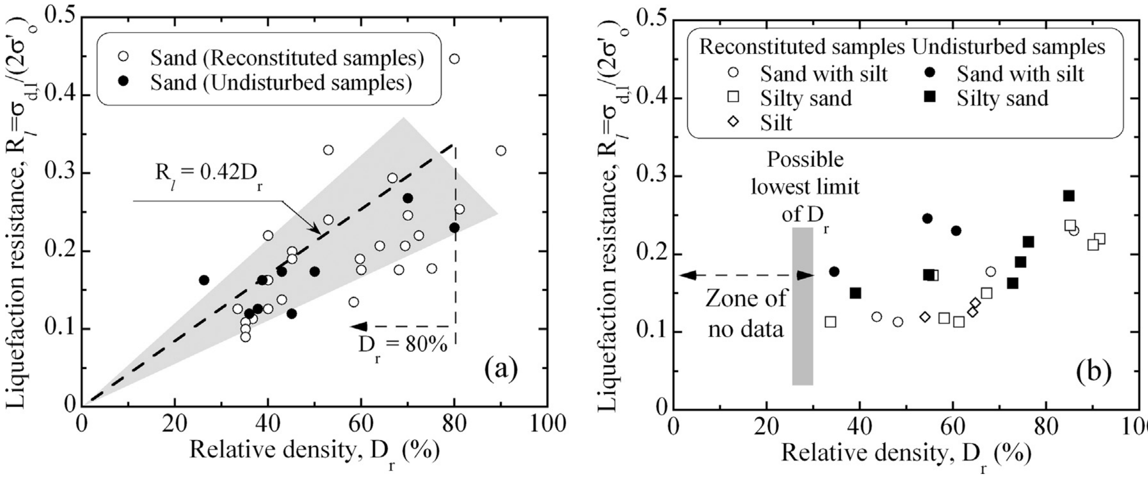

Fig. 4. Plots of saturated liquefaction resistance R_l against relative density D_r, (a) clean sand, (b) silty sand.

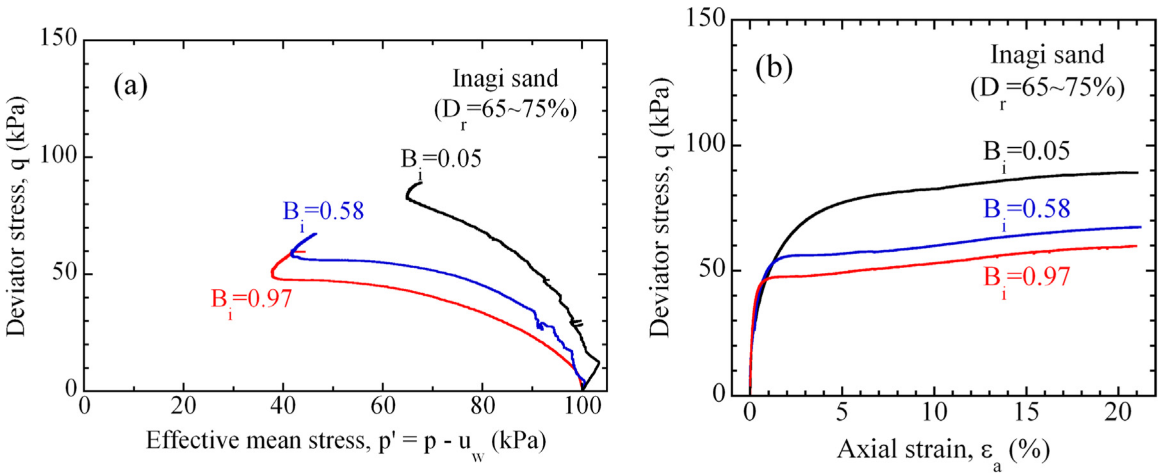

Fig. 5. Results of partially saturated undrained triaxial compression tests, (a) effective mean stress p′ – deviator stress q, (b) axial strain ε_a – deviator stress q, (Inagi sand, D_r = 65–75%).

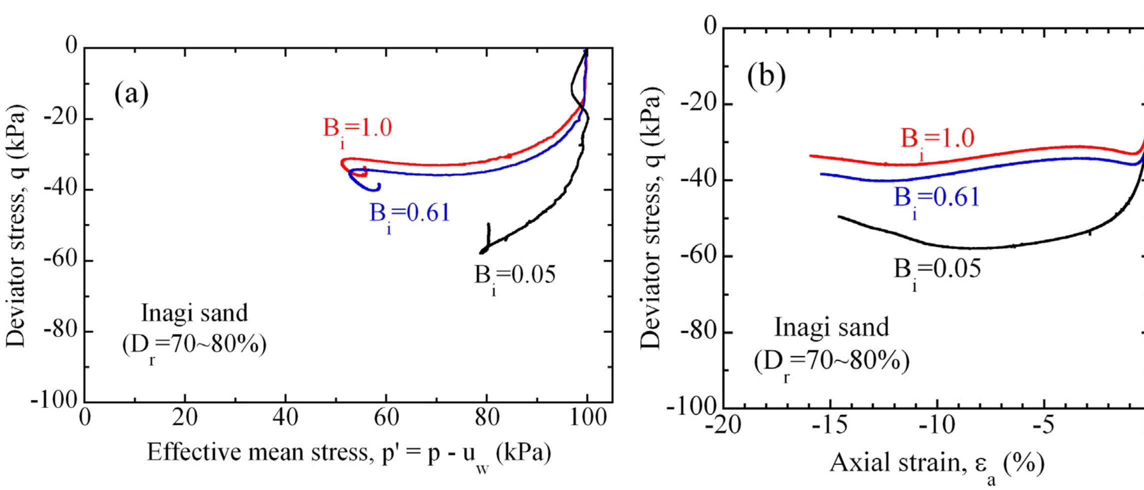

Fig. 6. Results of partially saturated undrained triaxial extension tests, (a) effective mean stress p′ – deviator stress q, (b) axial strain ε_a – deviator stress q, (Inagi sand, D_r = 70–80%).

values than the value of e_{min} determined from dry soil samples based on JGS [4]. It would be relevant to observe in Fig. 4(b) that no unique relation can be found between the liquefaction resistance and density. It would be again interesting to reexamine it in the context of skeleton void ratio.

3. Undrained shear strength and liquefaction resistance of partially saturated silty sands

In partial saturation, the coefficient of pore water pressure B was found to serve as an efficient parameter, which changes from B = 1–0.1

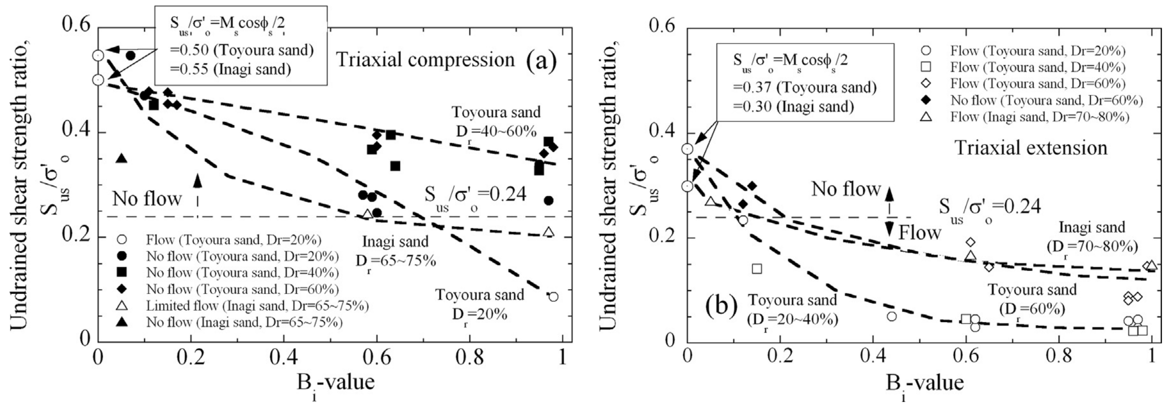

Fig. 7. Plots of partially saturated undrained shear strength ratio S_{us}/σ'_o against initial B_i-value, (Toyoura clean sand & Inagi silty sand), (a) triaxial compression, (b) triaxial extension.

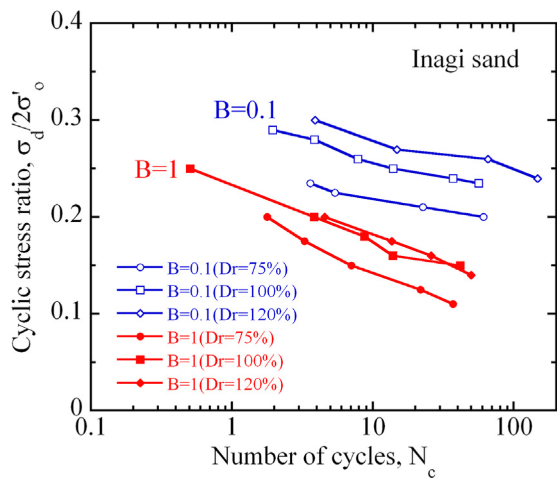

Fig. 8. Plots of cyclic stress ratio $\sigma_d/(2\sigma'_o)$ against number of cycles N_c in partially saturated undrained cyclic triaxial tests, (Inagi sand).

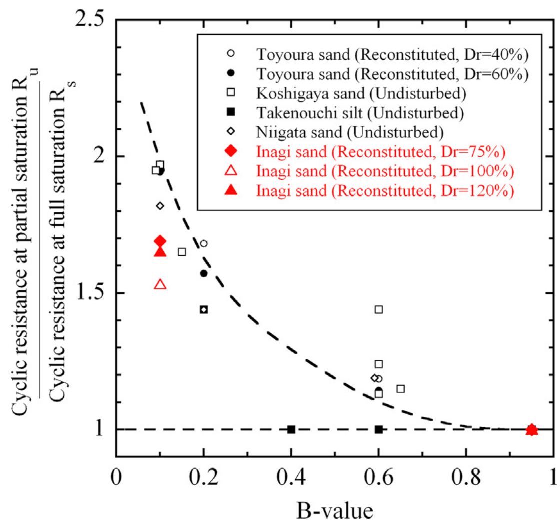

Fig. 9. Plots of ratios of partially saturated cyclic resistance R_u to fully saturated cyclic resistance R_s against B-value.

in response to the change in the degree of saturation S_r from 100% to 80%, as shown in Fig. 2. Since occluded tiny air bubbles are present within pore water in partial saturation and affect the compressibility of pore water, the B-value effectively measures a response of an excess pore water pressure to an overall change in all round confining pressure

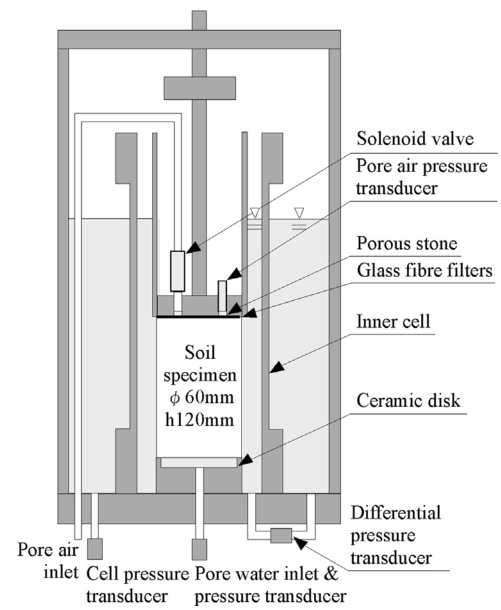

Fig. 10. Experimental setup of unsaturated triaxial tests.

acting on a soil specimen. In the previous study of Kamata et al. [2], the influence of partial saturation on the undrained triaxial compression and extension was examined for Toyoura clean sand. In this study, it is extended to Inagi silty sand. Those tests were conducted under a p-constant condition. The benefits arising from a p-constant condition were discussed by Tsukamoto et al. [5].

Fig. 5 shows the results of undrained triaxial compression tests on partially saturated Inagi sand. It is quite obvious to see in Fig. 5 that there would be only one unique failure envelope in p′-q plots, though the effective stress paths under different B-values differ significantly due to the difference in the developments of excess pore water pressures, which would be affected by the compressibility of pore water. In Fig. 6, the results of undrained triaxial extension tests are also shown. The data of the undrained shear strength S_{us} are then extracted from the test results shown in Figs. 5 and 6, and the values of undrained shear strength ratio S_{us}/σ'_o are plotted against the initial B-values (denoted as B_i hereafter) as shown in Fig. 7, together with the data on Toyoura sand obtained in the previous study. Herein, σ'_o is the initial effective confining stress, and the undrained shear strength is defined as $S_{us} = (q_s/2) \cos\phi_s$, where q_s is the deviator stress measured at phase transformation and ϕ_s is the internal friction angle determined from phase transformation line. It is observed in Fig. 7 that the relations between S_{us}/σ'_o and B_i, which are indicated as dashed curves, are rather dependent on

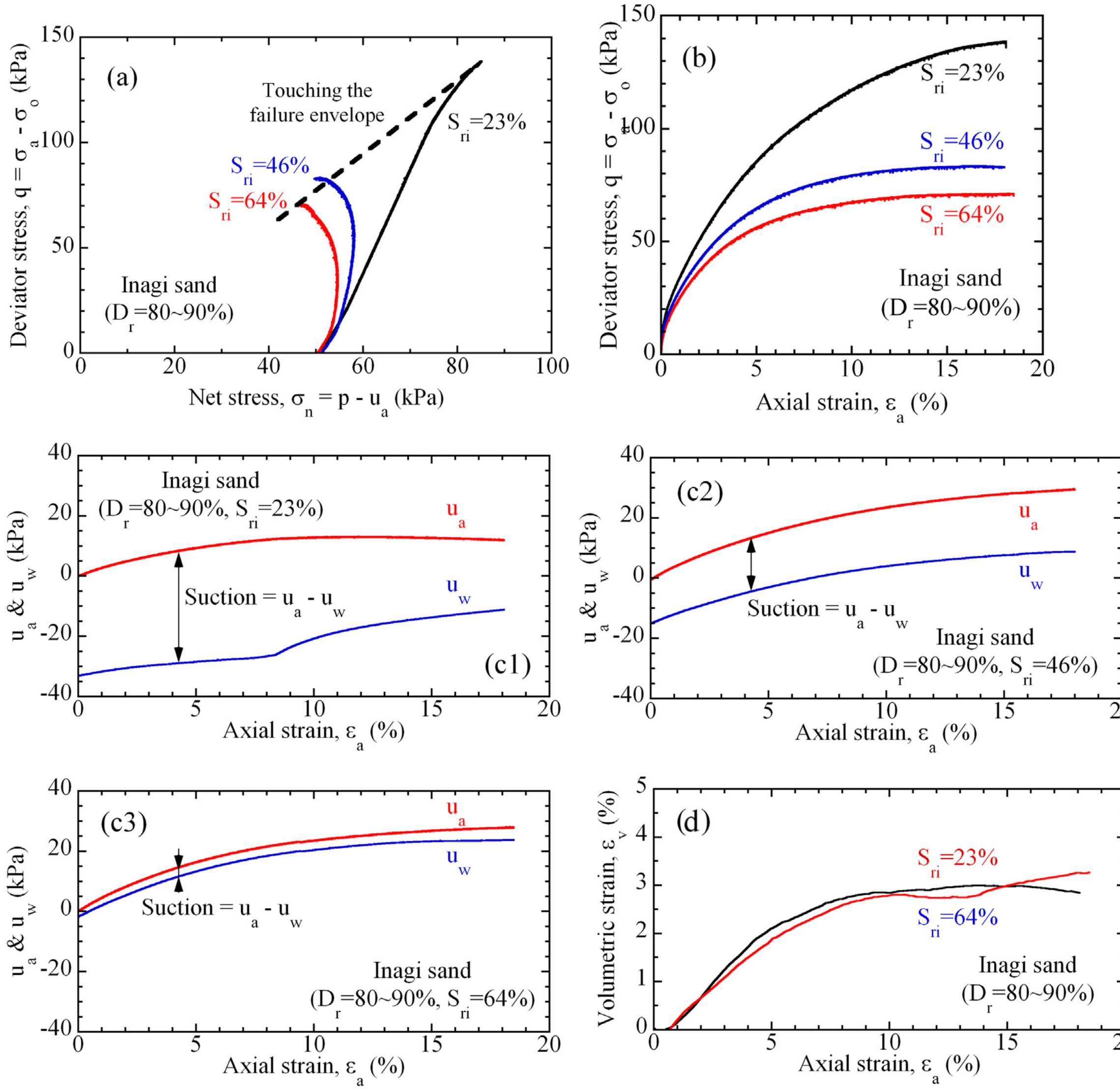

Fig. 11. Results of unsaturated undrained triaxial compression tests, (a) net stress σ_n = p-u_a – deviator stress q = σ_a-σ_o, (b) axial strain ε_a – deviator stress q, (c) axial strain ε_a – pore air and pore water pressures, u_a & u_w, (d) axial strain ε_a – volumetric strain ε_v, (Inagi sand, D_r = 80–90%).

density as well as soil types with different dilatancy characteristics. However, the threshold value of S_{us}/σ'_o = 0.24 dividing flow and no flow determined in full saturation also seems appropriate for partial saturation. It is interesting to see in Fig. 7 that there could definitely be presence of characteristic points at B_i = 0, which are defined by S_{us}/σ'_o = $(M_s/2)\cos\phi_s$, corresponding to a drained shear strength ratio exhibited under a p-constant condition. It is also found that when these sands are loose enough, flow slides could be triggered with the B-values greater than 0.7 in triaxial compression and with the B-values greater than 0.3 in triaxial extension.

The liquefaction resistances of partially saturated sands were extensively studied by Tsukamoto et al. [5], and were exercised in field studies with velocity logging tests by Nakazawa et al. [6]. In this study, it is extended to Inagi silty sand. Fig. 8 shows the values of cyclic stress ratio $\sigma_d/(2\sigma'_o)$ plotted against number of cycles N_c to achieve double amplitude axial strain $DA\varepsilon_a$ of 5%, which were obtained from a series of undrained cyclic triaxial tests on partially saturated Inagi silty sand. Those tests were conducted under two different B-values of 0.1 and 1 on the soil specimens with three different values of relative density D_r. The values of liquefaction resistance were then determined as the values of cyclic stress ratio $\sigma_d/(2\sigma'_o)$ observed at N_c = 20. Those data are then included in the plots of ratios of partially saturated cyclic resistance R_u to fully saturated cyclic resistance R_s against B-values as shown in Fig. 9, which were summarised in the previous study.

4. Undrained shear strength and cyclic resistance of unsaturated silty sands

Laboratory triaxial testing on unsaturated soils requires some specific devices as shown in Fig. 10, Tsukamoto et al. [7]). In separately regulating and monitoring pore air and pore water pressures, located at the bottom of a soil specimen in the pedestal is a water-saturated ceramic disk with an air entry value of 100 kPa, and located at the top of a soil specimen in the cap is a couple of glass fibre filters to cover the surface of small porous stones. The inner cell and differential pressure transducer are frequently used to directly monitor the volume change of an unsaturated soil specimen. The details of testing apparatus and procedure are described by Tsukamoto et al. [7]. The preparation of unsaturated soil specimens also should be undertaken with due care, to avoid any inhomogeneous pore water distributions in unsaturated soil specimens. In this study, the results on unsaturated Inagi silty sand are examined in more detail, which in part were previously discussed by Tsukamoto et al. [7]. In all of the tests discussed herein, the valves for both of the pore air and pore water tubes were closed to maintain the

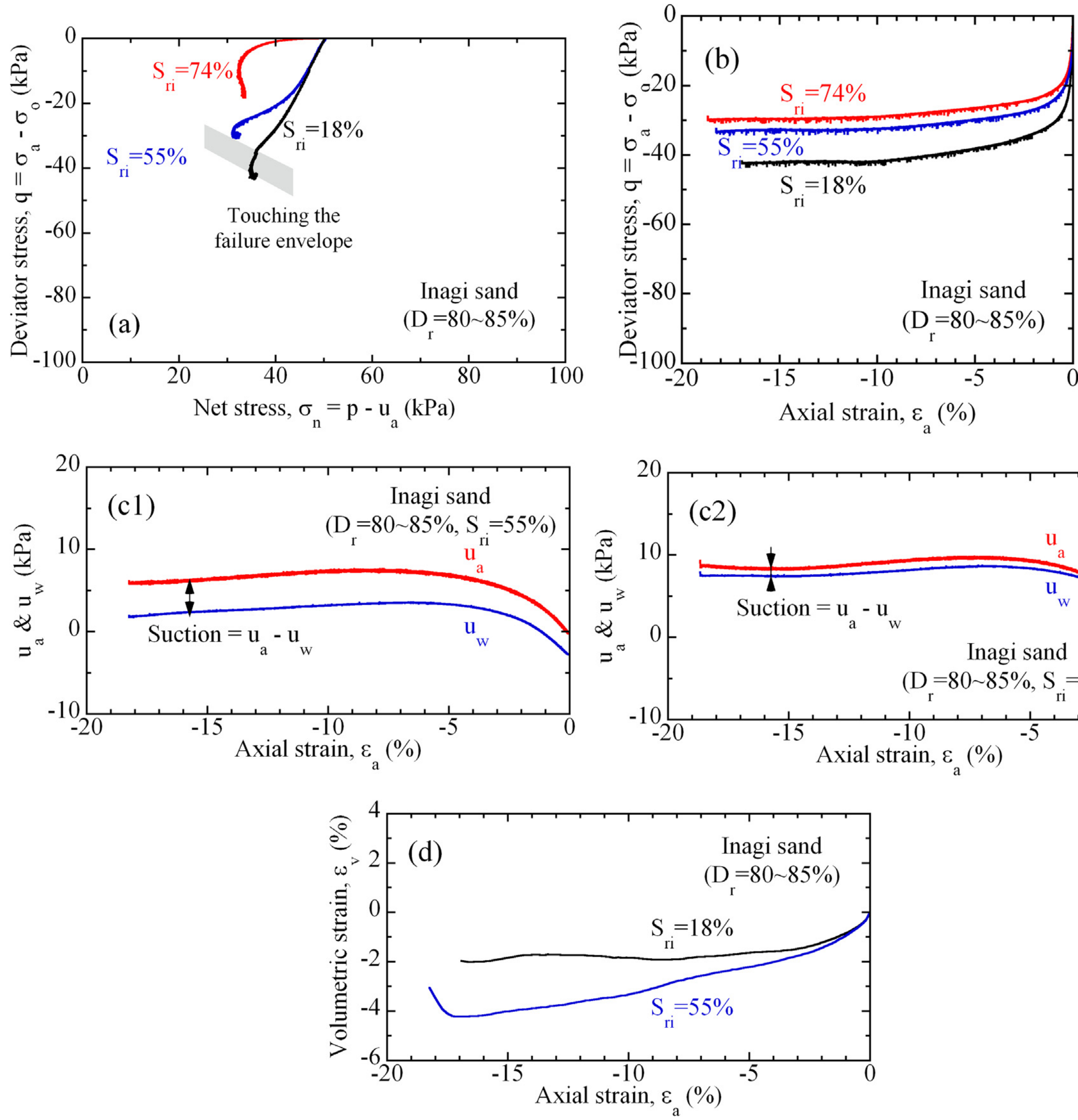

Fig. 12. Results of unsaturated undrained triaxial extension tests, (a) net stress σ_n =p-u_a – deviator stress q = σ_a-σ_o, (b) axial strain ε_a – deviator stress q, (c) axial strain ε_a – pore air and pore water pressures, u_a & u_w, (d) axial strain ε_a – volumetric strain ε_v, (Inagi sand, D_r = 80–90%).

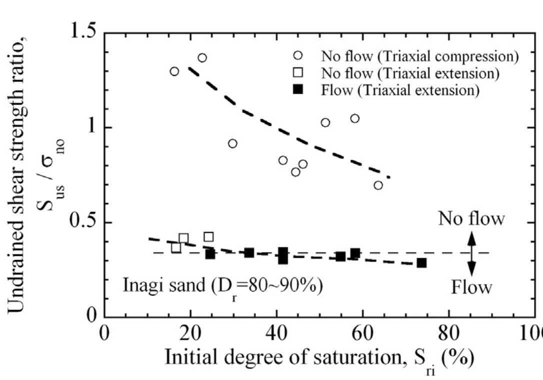

Fig. 13. Plots of unsaturated undrained shear strength ratio S_{us}/σ'_o against initial degree of saturation S_{ri}, (Inagi sand, D_r = 80–90%).

undrained condition for pore air and pore water.

Fig. 11 shows the results of undrained triaxial compression tests on unsaturated Inagi sand. Three series of tests under S_r = 23, 46, 64% are indicated. It is expected in Fig. 11(c) that larger values of initial matric suction, $S_u = u_a - u_w$, can be observed in the tests with lower values of degree of saturation S_r. However, the pore air pressure u_a and pore water pressure u_w tend to develop more greatly during triaxial compression in the tests with larger values of S_r. It is also seen in Fig. 11(d) that contractive volumetric strain ε_v can be observed during triaxial compression due mainly to compressibility of pore air. The pore air pressure buildup and volumetric contraction of unsaturated soil specimens are therefore the main consequences for unsaturated soil specimens subjected to triaxial compression. The difference in the pore air pressure buildup led to different undrained shear strengths which are defined from the deviator stress observed when the effective stress paths touched upon the failure envelope, as shown in Fig. 11(a). In Fig. 12, the results of undrained triaxial extension tests are shown. It is interesting to observe the pore air pressure buildup and volumetric dilation in case of triaxial extension. The data of deviator stress q_s observed at failure are then extracted from the test results shown in Figs. 11 and 12, and the values of undrained shear strength ratio are calculated as $S_{us}/\sigma_{no} = (q_s/2)\cos\phi_s/\sigma_{no}$. Herein, σ_{no} is the initial net stress at drained isotropic consolidation and is defined as $\sigma_n = \sigma_o - u_a$, where σ_o is the confining stress. Those data are plotted against initial degree of saturation S_{ri}, as shown in Fig. 13. It is interesting to see that the values of undrained shear strength ratio under triaxial compression are quite high, exhibiting “no flow” behaviour. However, those under

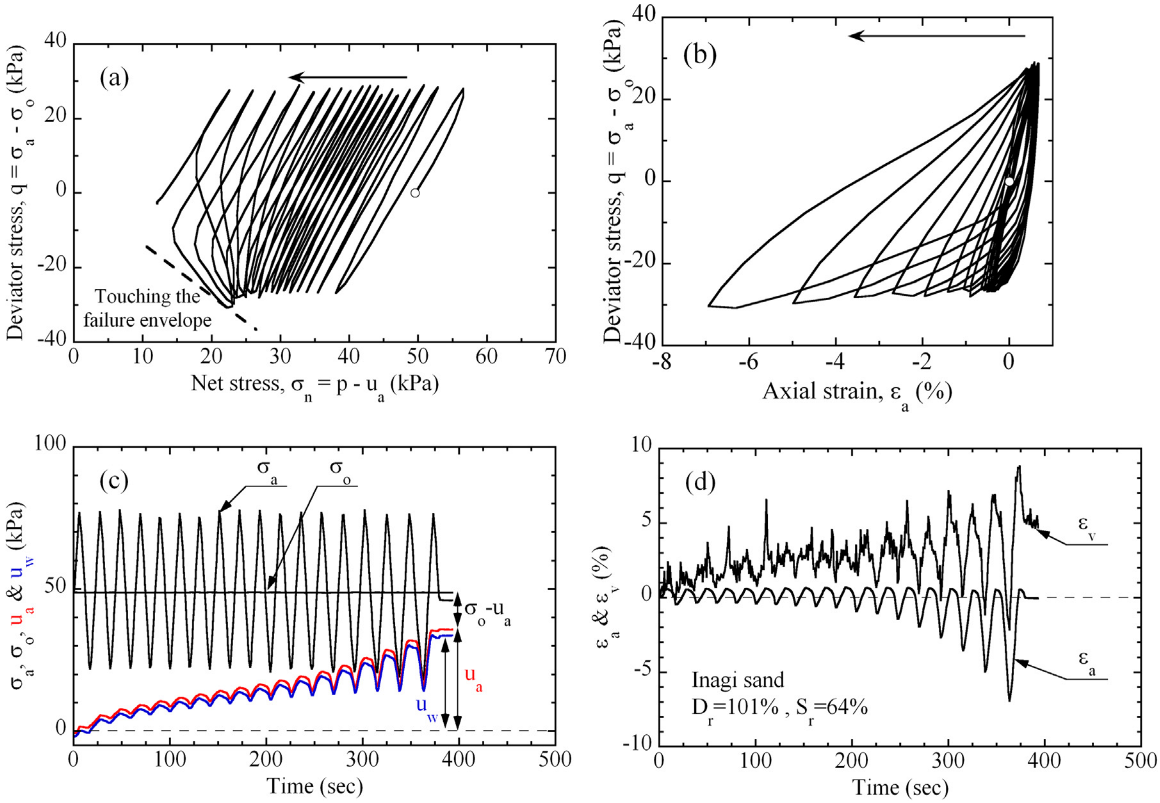

Fig. 14. Results of unsaturated undrained cyclic triaxial tests, (a) net stress σ_n = p-u_a – deviator stress q = σ_a-σ_o, (b) axial strain ε_a – deviator stress q, (c) time - axial stress σ_a, confining stress σ_o and pore air pressure u_a, (d) time - axial strain ε_a and volumetric strain ε_v, (Inagi sand, D_r =101%, S_r = 64%).

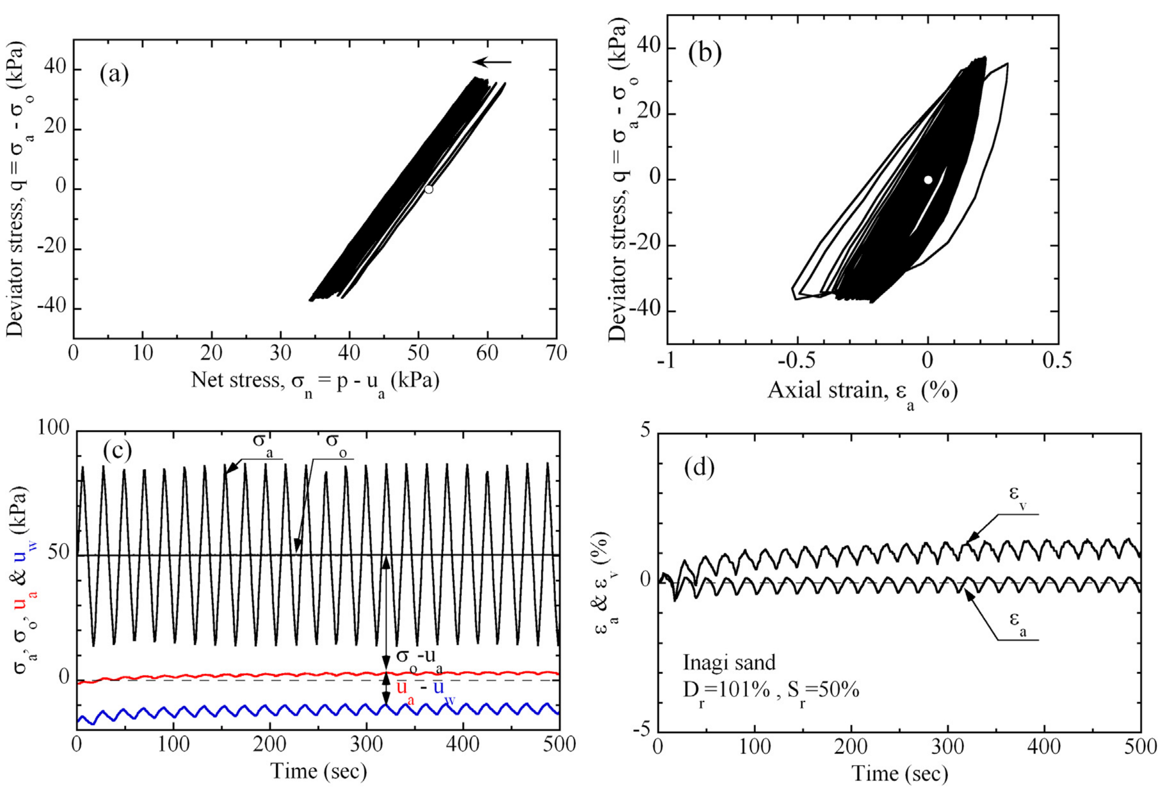

Fig. 15. Results of unsaturated undrained cyclic triaxial tests, (a) net stress σ_n = p-u_a – deviator stress q = σ_a-σ_o, (b) axial strain ε_a – deviator stress q, (c) time - axial stress σ_a, confining stress σ_o and pore air pressure u_a, (d) time - axial strain ε_a and volumetric strain ε_v, (Inagi sand, D_r = 101%, S_r = 50%).

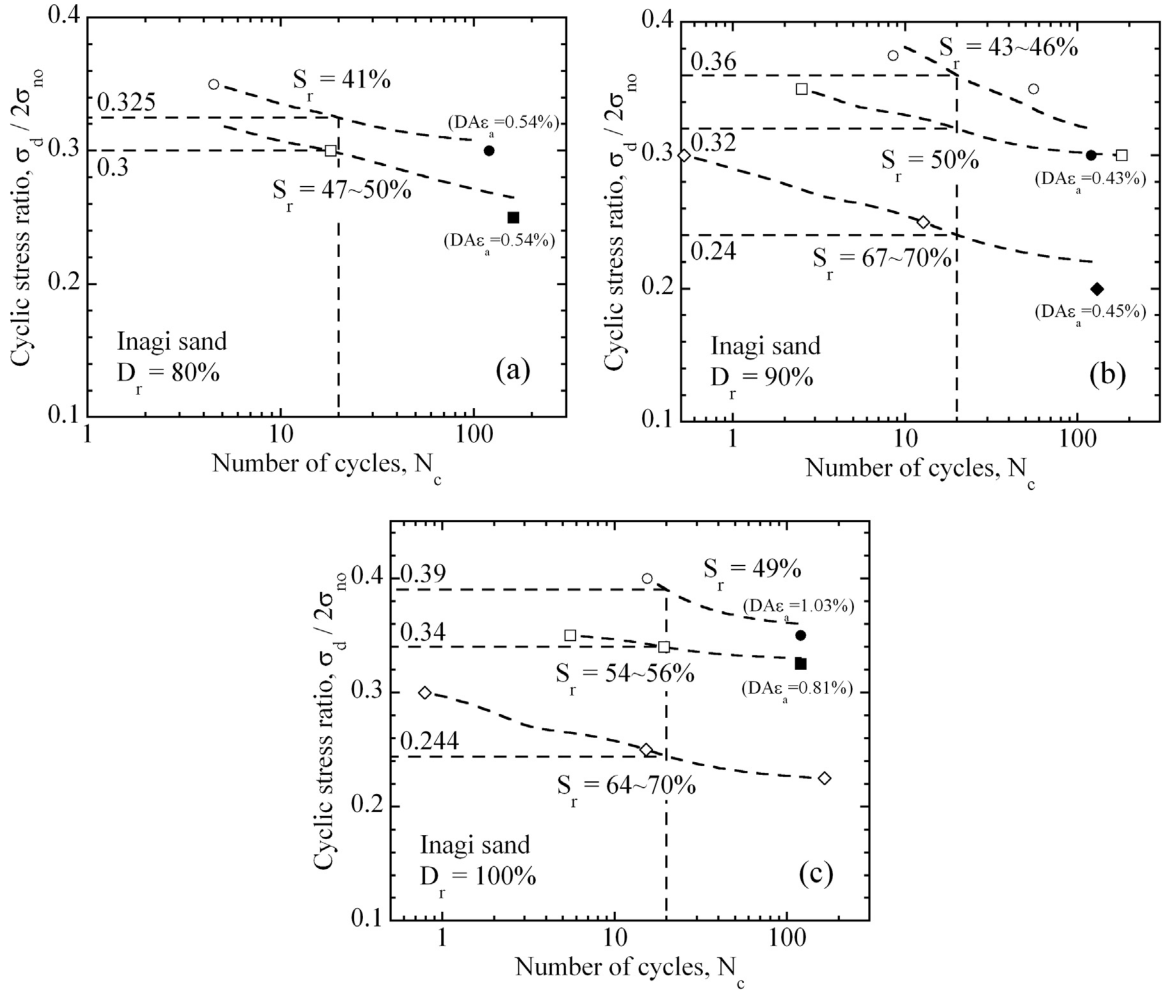

Fig. 16. Plots of cyclic stress ratio $\sigma_d/2\sigma_{no}$ against number of cycles, (Inagi sand), (a) D_r = 80%, (b) D_r = 90%, (c) D_r = 100%.

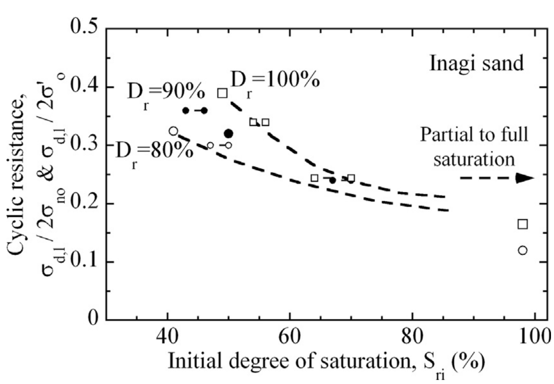

Fig. 17. Plots of unsaturated cyclic resistance $\sigma_{d,l}/2\sigma_{no}$ and saturated liquefaction resistance $\sigma_{d,l}/2\sigma'_o$ against S_{ri}, (Inagi sand).

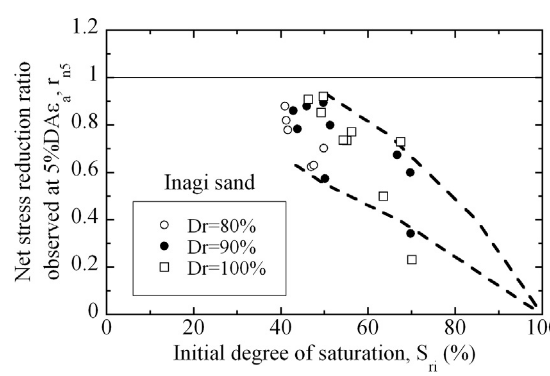

Fig. 18. Plots of net stress reduction ratio observed at 5%DAε_a, r_{n5}, against S_{ri}, (Inagi sand).

triaxial extension are quite low, and some of the nearly saturated tests with higher values of S_r exhibited “flow” behaviour, where the threshold value dividing flow and no flow can be estimated as S_{us}/σ_{no} = 0.35. Overall, flow slides could be triggered with the values of S_r greater than 60% in triaxial extension.

Fig. 14 shows the results of undrained cyclic triaxial tests on unsaturated Inagi sand with relatively higher degree of saturation S_r = 64%. The value of relative density D_r exceeds 100%, which occurs frequently for fines-containing sands due to the testing methods of determining e_{max} and e_{min} in dry conditions (JGS [4]). In Fig. 14(c), the pore air pressure u_a and pore water pressure u_w gradually increased during undrained cyclic loading, and compressive volumetric strain ε_v and extensional axial strain ε_a were observed as shown in Fig. 14(d). In Fig. 14(a), the effective stress path touched upon the failure envelope in triaxial extension, and consequently the axial strain rapidly developed as shown in the cyclic stress – stain relation of Fig. 14(b). In Fig. 15, the test results on Inagi sand with lower degree of saturation S_r = 50% are shown. When the degree of saturation is low enough, the pore air pressure u_a and pore water pressure u_w did not change significantly, neither did the volumetric strain ε_v and axial strain ε_a, as shown in Fig. 15(c) and (d). Therefore, the effective stress path did not touch upon the failure envelope, and the cyclic stress – stain relation did not

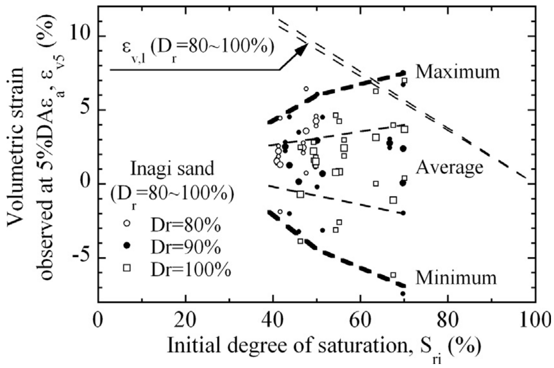

Fig. 19. Plots of volumetric strain observed at $5\%DA\varepsilon_a$, ε_{v5}, against S_{ri}, (Inagi sand).

move significantly, as shown in Fig. 15(a) and (b).

Based on multiple series of undrained cyclic triaxial tests on Inagi sand with D_r = 80%, 90% and 100%, which were saturated with different degrees of saturation S_r, the plots of cyclic stress ratio $\sigma_d/(2\sigma_{no})$ against number of cycles to achieve double amplitude axial strain $DA\varepsilon_a$ of 5% are produced as shown in Fig. 16. It is to note here that some of the tests did not even reach up to $DA\varepsilon_a$ of 5%. In such cases, the data points are provided as black symbols for reference in Fig. 16. From the extrapolations of the data points in Fig. 16, the values of cyclic resistance ratio $\sigma_{d,l}/(2\sigma_{no})$ are estimated as the cyclic stress ratio corresponding to N_c = 20, following the usual practice of liquefaction analysis, and plotted against S_{ri}, as shown in Fig. 17. The values of liquefaction resistance at full saturation $\sigma_{d,l}/(2\sigma'_o)$ are also plotted in Fig. 17. The significant reduction of cyclic resistance is observed with increasing degree of saturation in Fig. 17, particularly when the degree of saturation S_r reaches 60%.

Some other aspects of response of unsaturated sand to undrained cyclic loading are examined in Figs. 18 and 19. Fig. 18 shows the plots of net stress reduction ratio observed at $5\%DA\varepsilon_a$, r_{n5}, against S_{ri}. The net stress reduction ratio r_{n5} is defined as the net stress of $\sigma_n = \sigma_o - u_a$ observed at $5\%DA\varepsilon_a$ divided by the initial net stress σ_{no} equal to 50 kPa. There need to be two stress state variables for unsaturated soils, net normal stress $(\sigma - u_a)$ and matric suction $(u_a - u_w)$, (Fredlund and Rahardjo [1]). It was found in Figs. 14 and 15 that the net normal stress $(\sigma - u_a)$ changes quite rapidly during undrained cyclic loading, though the matric suction $(u_a - u_w)$ does not change so significantly. The significant reduction of the net normal stress can be observed as the degrees of saturation are raised higher than S_r = 60–70%. Fig. 19 shows the plots of volumetric strain observed at $5\%DA\varepsilon_a$, ε_{v5}, against S_{ri}. Since the values of volumetric strain fluctuated significantly during undrained cyclic loading, the maximum, minimum and average values observed at $5\%DA\varepsilon_a$ are all plotted in Fig. 19. Herein, the liquefaction-inducing volumetric strain $\varepsilon_{v,l}$ assumed by Unno et al. [8] can be examined, which is defined as follows.

$$\varepsilon_{v,l} = \left(1 - \frac{u_{ao\,abs}}{\sigma_{o\,abs}}\right) \times \frac{e(1 - Sr)}{1 + e} \tag{2}$$

where u_{ao_abs} and σ_{o_abs} are the initial pore air pressure and the confining stress, defined both in absolute pressures. The relation of Eq. (2) is also plotted in Fig. 19. It is found in Fig. 19 that the maximum values of volumetric strain begin to approach the liquefaction-inducing volumetric strain $\varepsilon_{v,l}$ as the degrees of saturation become larger than about S_r = 60–70%. Based on the discussions associated with the reductions of cyclic resistance and net normal stress as well as the development of volumetric strain critically approaching the liquefaction-inducing volumetric strain $\varepsilon_{v,l}$, that are shown in Figs. 17, 18 and 19, it would be relevant to assume that liquefaction-like unstable phenomena would occur as the degree of saturation becomes larger than S_r = 60–70% for Inagi sand.

5. Conclusions

The undrained shear strength and liquefaction cyclic resistance of silty sands were examined and discussed separately in the three phases of full saturation, partial saturation and unsaturation, based on a large number of laboratory triaxial test results. The past studies of the authors' were reviewed and some new data were added where appropriate.

In full saturation, the largest value of undrained shear strength ratio causing "flow" is 0.24. In partial saturation, the ranges of B-value causing "flow" are different for triaxial compression and extension. The condition of "flow" occurs under the B-value greater than 0.7 in triaxial compression and those greater than 0.3 in triaxial extension. In unsaturation, the condition of "flow" only occurs under the value of S_r greater than 60% in triaxial extension.

Partial saturation and unsaturation lead to the apparent increase of liquefaction resistance up to 2–3 times greater than full saturation.

Overall, those three phases were found to yield to distinctly different responses of silty sands and led to different characteristics in the undrained shear strength and liquefaction cyclic resistance.

Acknowledgements

The author acknowledges the kind support and encouragement from Professor K. Ishihara. The laboratory tests presented in this study were conducted by the past students of Tokyo University of Science, including M. Inami and J. Matsumoto.

References

[1] Fredlund DG, Rahardjo H. Soil Mechanics for Unsaturated Soils. A Wiley-Interscience Publication. New York: John Wiley & Sons; 1993.
[2] Kamata T, Tsukamoto Y, Ishihara K. Undrained shear strength of partially saturated and in triaxial tests. Bull N Z Soc Earthq Eng 2009;42(1):57–62.
[3] Tsukamoto Y, Ishihara K, Kamata T. Undrained shear strength of soils under flow deformation. Geotechnique 2009;59(5):483–6.
[4] Japanese. Geotechnical Society Testing methods and interpretations of geotechnical laboratory experiments. Japanese Geotechnical Society. Tokyo (in Japanese); 2000.
[5] Tsukamoto Y, Ishihara K, Nakazawa H, Kamada K, Huang Y. Resistance of partly saturated sand to liquefaction with reference to longitudinal and shear wave velocities. Soils Found 2002;42(6):93–104.
[6] Nakazawa H, Ishihara K, Tsukamoto Y, Kamata T. Case studies on evaluation of liquefaction resistance of imperfectly saturated soil deposits. Proceedings of International Conference on Cyclic Behaviour of Soils and Liquefaction Phenomena, Bochum. Germany; 31 March – 02 April 2004; Cyclic Behaviour of Soils and Liquefaction Phenomena (ed. Th. Triantafyllidis): 295–304. Taylor & Francis Group. London.
[7] Tsukamoto Y, Kawabe S, Matsumoto J, Hagiwara S. Cyclic resistance of two unsaturated silty sands against soil liquefaction. Soils Found 2014;54(6):1094–103.
[8] Unno T, Kazama M, Uzuoka R, Sento N. Liquefaction of unsaturated sand considering the pore air pressure and volume compressibility of the soil particle skeleton. Soils Found 2008;48(1):87–99.